Mathematical Biology

Clare L. Chapman · James J. Wright · Paul D. Bourke

Spatial eigenmodes and synchronous oscillation: Co-incidence detection in simulated cerebral cortex

Abstract. Zero-lag synchronisation arises between points on the cerebral cortex receiving concurrent independent inputs; an observation generally ascribed to nonlinear mechanisms. Using simulations of cerebral cortex and Principal Component Analysis (PCA) we show patterns of zero-lag synchronisation (associated with empirically realistic spectral content) can arise from both linear and nonlinear mechanisms.

For low levels of activation, we show the synchronous field is described by the eigenmodes of the resultant damped wave activity. The first and second spatial eigenmodes (which capture most of the signal variance) arise from the even and odd components of the independent input signals. The pattern of zero-lag synchronisation can be accounted for by the relative dominance of the first mode over the second, in the near-field of the inputs. The simulated cortical surface can act as a few millisecond response coincidence detector for concurrent, but uncorrelated, inputs.

As cortical activation levels are increased, local damped oscillations in the gamma band undergo a transition to highly nonlinear undamped activity with 40 Hz dominant frequency. This is associated with "locking" between active sites and spatially segregated phase patterns.

The damped wave synchronisation and the locked nonlinear oscillations may combine to permit fast representation of multiple patterns of activity within the same field of neurons.

1. Introduction and background

Synchronisation has been suggested as a solution to the binding and segregation problems of psychology [4,5,13–15,23–25,29,31,40,62]. Object features might be bound by synchronous neuronal firing and coded for by spatially separated cells or cell assemblies in the cortex [59]. The phase differences between sets of these distributed synchronous firing cells might code multiple objects in the system [61].

C.L. Chapman: School of Mathematics and Statistics F07, University of Sydney, NSW 2006, Australia. e-mail: clarec@maths.usyd.edu.au

J.J. Wright: c/o Liggins Institute University of Auckland Medical School, Park Road, Grafton, Auckland, New Zealand. e-mail: jjw@mhri.edu.au

P.D. Bourke: Centre for Astrophysics and Computing, Swinburne University of Technology, Hawthorne, Victoria 3122, Australia. e-mail: pbourke@swin.edu.au

Empirical verification of gamma band stimulus–induced synchronisation in the brain has been found in single unit and multiunit local field potential (LFP) and electroencephalogram (EEG) recordings [4, 13, 15, 23–25].

There is no universally accepted mechanism to account for all the experimental evidence for synchronous activity in the brain. Doubts have also been raised as to whether such synchronisation is relevant to binding or segregation [43]. Such doubts include uncertainties about the time–window for synchronisation, the degree to which synchronisation can shift time differences between neural events and, particularly, the time it takes to establish synchronisation in ongoing activity [8]. This paper attempts to account for synchronous behaviour in simple physical terms.

Distinction is made between *zero–lag synchrony* and *synchronous oscillation*. Zero–lag synchrony (synchrony for short) is defined as high positive linear cross–correlation/covariance at zero phase–lag between separate sites in cortex. Synchrony is generally associated with damped sinusoidal or nonsinusoidal cross–correlation and auto–correlation functions [13, 15, 16, 23] but constant and slight or even negative damping profiles have been found [16, 34].

Synchronous oscillation, on the other hand, is synchronisation associated with gamma band EEG oscillations and found predominantly at 40 Hz. It has often been assumed that all synchronisation in the brain is a highly nonlinear phenomenon [1] since neuron firing is nonlinear at crucial stages of signal transmission [27]. Hence, large arrays of nonlinear neuron–like oscillators have been used to model cortical tissue and the observed nonlinear phase–locking in such models has been seen as the inevitable mechanism for global synchronisation in the cortex [6, 7, 10–12, 14, 18, 32, 35, 36, 52, 56–58] There is, however, conflicting evidence [61] such as observations of broad band synchronisation [4] and synchronous activity seen in continuum models of electrocortical behaviour which do not depend on essential nonlinearity [48, 67, 68].

The models of electrocortical activity used in this paper subsume individual properties into a collective mass action. This *continuum* framework produces waves almost akin to linear superposition waves which are associated with synchrony [48, 67] as well as synchronous oscillation. A full discussion of these models and experimental findings can be found in a recent review [66]. The term continuum as it is used here specifically refers to the act of lumping together the activity of a group of neurons and treating them as an entity rather than referring to mathematical continuity. The numerical model utilised here is discrete rather than continuous. Properties and formulation of a partial differential version of the present discrete, and integral, model have been explored elsewhere [46, 48].

In this paper we use cross–correlation methods to demonstrate synchrony in a simplified averaging model and cross–correlation and PCA methods to show synchrony, synchronous oscillation and nonlinear phase–locking within a realistic physiological model. We show the synchrony mechanism is a form of coincidence detection, or selective filtering of input signals, with very rapid onset and this essentially linear mechanism gives way to non–linear phase–locked synchronous oscillation, within the 40 Hz band in the realistic physiological model.

2. Analysis tools

The cross–correlation coefficient ρ between two LFP time series, is:

$$\rho(i, j) = \frac{c(i, j)}{\sqrt{c(i, i)c(j, j)}} \tag{1}$$

where $c(i, j)$ is the covariance between the ith and jth time series. If, as here, all elements are measured in the same units then covariance alone can be used in the PCA. The method involves calculation of the eigenvectors $\mathbf{e_i}$ and eigenvalues λ_i of the covariance C matrix of the m state–variable system. The system matrix, Z for n time steps is:

$$\mathbf{Z} = \begin{bmatrix} z(1, 1) & z(1, 2) & \ldots & z(1, m) \\ z(2, 1) & z(2, 2) & \ldots & z(2, m) \\ \vdots & & & \vdots \\ z(n, 1) & z(n, 2) & \ldots & z(n, m) \end{bmatrix} \tag{2}$$

where $z(i, j)$ is the system value with temporal mean removed at spatial position j at time i. The covariance:

$$\mathbf{C} = \frac{1}{(n-1)}\mathbf{Z}^T\mathbf{Z} \tag{3}$$

satisfies the eigenvalue equation:

$$\mathbf{C}\mathbf{e}_i = \lambda_i\mathbf{e}_i \tag{4}$$

with the temporal principal component vector for each eigenvector given by:

$$\mathbf{a}_j = \mathbf{Z}\mathbf{e}_j \tag{5}$$

3. Models

Two simulation models are used; a simplified dendritic averaging model and a physiological model [65]. We begin with the simple model.

3.1. Simplified averaging model

The averaging model consists of positive–feedback linked linear elements and was used to specify minimum requirements for synchronisation. Connectivity strength between elements was weighted by a Gaussian function of distance. For a distance r_{pq} between elements p and q the weighting was:

$$\omega_{pq} \propto e^{-\frac{1}{2}(\frac{r_{pq}}{\sigma})^2} \tag{6}$$

A given element's input was composed of the V_{out} of other elements weighted by this connection strength, with σ the standard deviation. The time δt_{pq} it took voltage signals $V_{out}(t)$ to travel this distance was dependent on r_{pq} and axonal transmission speed v so:

$$\delta t_{pq} = \frac{r_{pq}}{v} \tag{7}$$

The voltage at the *pth* element at time t_0 was then:

$$V_{in}^{(p)}(t_0) = \sum_{q=1}^{m} \omega_{pq} V_{out}^{(q)}(t_0 - \delta t_{pq}) \tag{8}$$

A particular lumped element's voltage can be modelled as a summation of earlier voltage values due to the delays and fall-off characteristics associated with dendritic potentials. For N time steps (with length of time step $\triangle t$) this dendritic potential summation is:

$$V_{out}^{(p)}(t_0) = \frac{\sum_{i=1}^{N} V_{in}^{(p)}(t_0 - i\triangle t)}{2N} \tag{9}$$

3.2. Physiological model

The model used here (reported in detail elsewhere [68]) is an intermediate stage in a family of models [44–48, 66, 67] which progress from the simplest possible descriptions of the cortex as a delay network. By introducing more complex aspects of cerebral dynamics and independently specified parameter values in a step-wise fashion we aim for an increasingly accurate account of cerebral dynamics [66]. The level of development used here is sufficient to reproduce the essential features of synchronous oscillation [65]. The spectral properties observed (notably the capacity for oscillation in the gamma and 40 Hz range) are dependent on rapid feedback processes operating at synaptic level. Justifications for the use of normalised units, and for the particular parameter values here applied, are given in the earlier papers [30, 33, 42, 51, 53, 68]. These values, and the match to experimental data have been improved in subsequent stages of development of the family of models, but no essential change in the class of dynamics here described is brought about by the later modifications.

3.3. State-equations

This model represents the continuum of cortical tissue as discrete cortical zones in the spirit of Wilson and Cowan [63, 64]. Transfer of afferent synaptic impulses to efferent pulses via dendritic processes is modelled by a biexponential lag function matched to physiological measurements [45, 53, 54].

The N cells in unit volume each have a probability of emission of an action potential q_i as a function of their membrane potentials. The sum of population membrane potentials is directly proportional to the LFP, $V(t)$ at time t. Then in a mean-field approximation the pulse-probability density $Q(t)$ is given by:

$$Q = \frac{1}{N} \sum_{i=1}^{N} q_i(V) \tag{10}$$

By the central limit theorem, for large N, Q will have a Gaussian distribution with respect to V, independent of individual distributions of q_i, so V and Q are approximately related by:

$$Q = (1 + e^{a(V-3)})^{-1} \tag{11}$$

Where $a = -\pi/\sqrt{3}$, LFP voltage units (vu) are approximate to standard deviations of the distribution of cell pulse probability over the complete range of LFP, with a 50% mean probability of pulse emission 3 standard deviations from complete polarisation of the neural population.

The time response of mean membrane potential (and by implication LFP and soma potential) is given by

$$V(t) = g \sum_{j=1}^{n} w_j Q_a(t - j\Delta t) \quad j = 1, 2, 3...n \tag{12}$$

where g is synaptic gain, Q_a is afferent pulse action density, Δt is the discrete time-step, and $n\Delta t$ is large compared to the peak time response of membrane potential. In accord with [46]

$$w_j = b^2 j \Delta t e^{-bj\Delta t} \tag{13}$$

models the rise and fall of membrane potential in response to input at $t = 0$; incorporating lags due to both synaptic conduction and average dendritic cable delay in a single function. Parameter b regulates both the peak time and mean delay associated with this lag. Time step Δt was set at 0.1 ms, after trials showed progressive decrements of time-step to 0.01 ms produced only small, asymptotically diminishing effects on spectral content of the results.

Within unit volumes both excitatory and inhibitory cell groups are distinguished, each reciprocally and self-coupled, and each coupled at longer range to other unit volumes by cortico-cortical fibres. Delays due to axonal conduction between unit volumes are given by $\Delta\tau = r_{pq}/\nu$, where $\Delta\tau$ is axonal conduction lag over the distance r_{pq} between the pth unit volume and the qth unit volume and axonal conduction velocity is ν.

Coupling strengths are proportional to:

– The fractional density of synaptic couplings afferent to dendrites of excitatory and inhibitory cells respectively (α_{ee}, β_{ei}, μ_{ei}, M_{ee} etc., as listed in Table 2).
– The synaptic gains of excitatory and inhibitory synapses, g_e and g_i
– Changes in synaptic efficacy, E', representing feedback effects including those of reversal potentials [30]. These feedback relations are modelled as linear regressions of efficacy with membrane potential

$$
\begin{aligned}
E'_{ee}(t) &= (1 - V_{e(p)}(t - \Delta t)/V_{eR}) \\
E'_{ei}(t) &= (1 - V_{i(p)}(t - \Delta t)/V_{eR}) \\
E'_{ie}(t) &= (1 - V_{e(p)}(t - \Delta t)/V_{iR}) \\
E'_{ii}(t) &= (1 - V_{i(p)}(t - \Delta t)/V_{iR})
\end{aligned}
\tag{14}
$$

Subscripts e and i indicate excitatory and inhibitory potentials; subscript R a constant-valued reversal potential. Smoothed efficacies $\{E'\}$ were applied so $E(t) = \sum_{j=1}^{n} u_j E'(t - j\Delta t)$ where $u_j = ce^{-cj\Delta t}$. For large c, decay is rapid; analogous to reversal potentials alone.

State equations for the pth unit volume of the cortical system are then:

$$
\begin{aligned}
Q_{e(p)} &= (1 + e^{a(V_{e(p)}-3)})^{-1} \\
Q_{i(p)} &= (1 + e^{a(V_{i(p)}-3)})^{-1} \\
V_{e(p)} &= \sum_{j=1}^{n} w_j Q_{ae(p)}(t - j\Delta t) \\
V_{i(p)} &= \sum_{j=1}^{n} w_j Q_{ai(p)}(t - j\Delta t)
\end{aligned}
\tag{15}
$$

$Q_{ae(p)}$, $Q_{ai(p)}$ are pth unit volume afferent synaptic action densities for excitatory and inhibitory cells which receive local synaptic input (at negligible axonal delay) and delayed cortico-cortical inputs from qth unit volumes at range r_{pq}, $q = 1...u$. in accord with:

$$
\begin{aligned}
Q_{ae(p)} &= g_e \beta_{ee} E_{ee(p)} Q_{e(p)} - g_i \beta_{ie} E_{ie(p)} Q_{i(p)} \\
&\quad + g_e M_{ee} E_{ee(p)} Q_{s(p)} + g_e \mu_{ee} E_{ee(p)} Q_{ns(p)} \\
&\quad + g_e \sum_{1}^{u} \alpha_{ee}(r_{pq}) E_{ee(p)} Q_{e(q)}(t - r_{pq}/v) \\
Q_{ai(p)} &= g_e \beta_{ei} E_{ei(p)} Q_{e(p)} - g_i \beta_{ii} E_{ii(p)} Q_{i(p)} \\
&\quad + g_e M_{ei} E_{ei(p)} Q_{s(p)} + g_e \mu_{ei} E_{ei(p)} Q_{ns(p)} \\
&\quad + g_e \sum_{1}^{u} \alpha_{ei}(r_{pq}) E_{ei(p)} Q_{e(q)}(t - r_{pq}/v)
\end{aligned}
\tag{16}
$$

$\alpha_{ee}(r_{pq})$ and $\alpha_{ei}(r_{pq})$ are partial input synaptic densities. $\sum_{1}^{u} \alpha_{ee}(r_{pq}) = \alpha_{ee}$ and $\sum_{1}^{u} \alpha_{ei}(r_{pq}) = \alpha_{ei}$. Q_s and Q_{ns} are system inputs; Q_s represents all time-varying components in specific cortical afferents and Q_{ns}, acting as a control parameter, is a uniform DC input modelling nonspecific cortical activation. See [44] for analysis on the physics of this class of models.

3.4. Configuration of simulation

In both the simplified averaging and physiological models studied here an extended area of cortex was simulated by unit volumes in a 20 x 20 or 20 x 40 matrix, each volume connected with its neighbors so the coupling strengths, $\alpha_{ee}(x, y)$ declined with r_{pq} as a Gaussian function with standard deviation of 4 distance units. A distance unit was the side of one cell of the given matrix and $m = 400$ or 800 in equation (2). This approximates the distribution of cortico-cortical fibres in cat brain if the distance unit is taken as about 0.9 mm. Boundary conditions were toroidal in all simulations. Absorbing boundary conditions and matrix size changes did not qualitatively affect the reported results.

3.5. Parameter values

Model parameters are given in Tables 1 and 2.

4. Methods and results

Methods and results are presented together, since the latter methods are contingent on the earlier results.

A time step of $\Delta t = 0.1$ milliseconds allowed a 10000 Hz maximum sampling frequency; far more than needed to capture model frequencies – mainly below 100 Hz. Non-decimated data was retained for analysis to facilitate study of temporal precision in the full model.

Table 1. State-variables and standard parameters other than synaptic densities. LFP = local field potential, PPD = pulse probability density.

V_e	Excitatory LFP	vu
V_i	Inhibitory LFP	vu
Q_e	Excitatory PPD	Dimensionless
Q_i	Inhibitory PPD	Dimensionless
a	Slope parameter	$-\pi/\sqrt{3}\,(\text{vu}^{-1})$
b	Dendritic time-constant	$50\ \text{s}^{-1}$
g_e	Excitatory gain	65 vu
g_i	Inhibitory gain	260 vu
c	Decay time-constant.	$1000\ \text{s}^{-1}$
v	Axonal velocity	$9\ \text{m s}^{-1}$
$\sqrt{\overline{r^2_{pq}}}$	SD of axonal range	4 mm
V_{eR}	EPSP reversal	12 vu
V_{iR}	IPSP reversal	-0.02 vu
Q_{ns}	Nonspecific input	Dimensionless
Q_s	Specific input	Dimensionless

4.1. Simplified averaging model

Each lattice element started with a pulse density of zero. Two linearly uncorrelated *driving* noise inputs with 0.0 mean [37,41] and standard deviation 10.0 were given to the lattice at row 11 in columns 8 and 14. The two noise signals are referred to as an asynchronous noise source.

   The system was allowed to attain stationary temporal evolution about a steady state mean. Then multichannel data sets of length 20000 were generated for a range of summations in equation (9). Using a reference channel located at column 11 on

Table 2. Synaptic couplings subscripts *ee*, *ei*, *etc.*, indicate synapses between cell types, excitatory to excitatory, excitatory to inhibitory, etc. Types of coupling are: α (cortico-cortical connections), β (intracortical connections), μ (nonspecific cortical afferents) and M (specific afferents). Synaptic density fraction is the proportion of synapses of each type in unit cortical volume. (The exact values used in the simulations are given for completeness although the precision given is greater than is justified from the anatomical data.) Afferent fraction is the proportion of synapses on the excitatory or inhibitory cell dendrites respectively.

Synaptic coupling	Synaptic density fraction	Afferent fraction
α_{ee}	0.765	0.8693
β_{ee}	0.0845	0.0960
β_{ei}	0.0149	0.1242
α_{ei}	0.100	0.8333
β_{ie}	0.0228	0.0259
β_{ii}	0.004	0.0333
μ_{ee}	0.0077	0.0088
μ_{ei}	0.0011	0.0092
$M_{ee,i}$	Not given	

the 13th row of the lattice, calculations of maximum cross–correlation for 100 timesteps into the future and past were made for each channel in the lattice. The delay at which the maximums occurred was also noted. The process was repeated for a selection of noise seeds and a typical case is plotted in Figure 1.

As summation length increased a pattern of maximum cross–correlation in elements around the driving sites developed. Results are calculated from the analogue of LFP but, equivalently, could be obtained using pulse–density as the observed state variable. A comparison of all cases showed the synchronous field was most highly developed for $N = 100$, where a maximum correlation close to 1.0 was
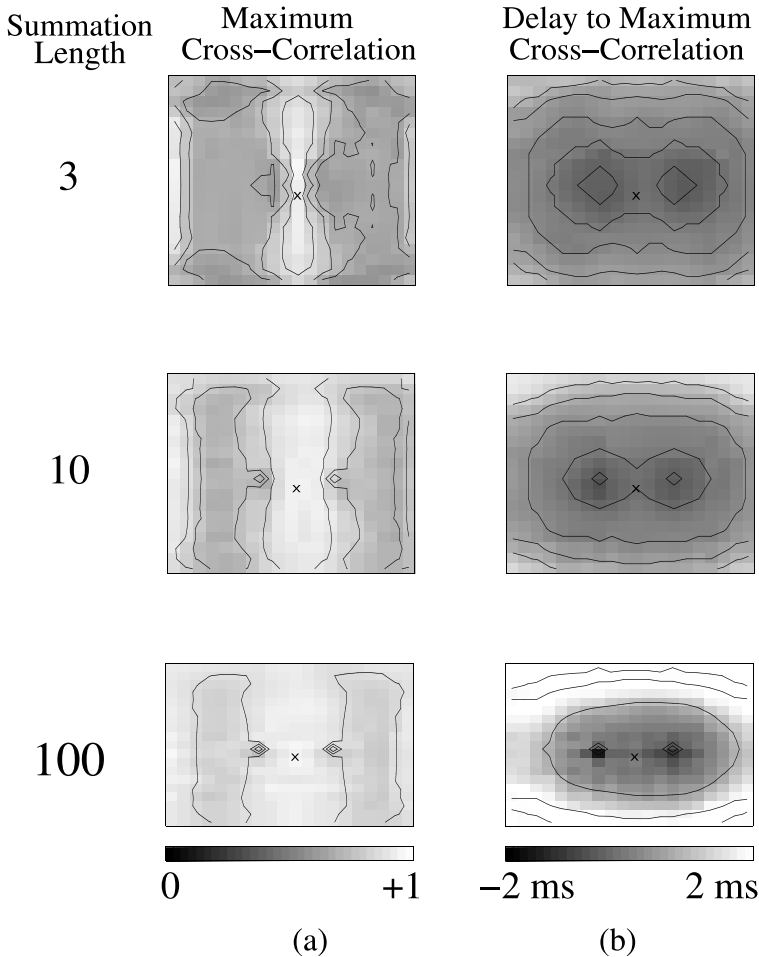

Fig. 1. Cross–correlation results for 20 x 20 version of Simplified Averaging model with two driving sites (see text) input asynchronous Gaussian noise. (a) Grey scale spatial plots of maximum cross–correlation, of the site marked 'x', with every other site for lags of ±100 timesteps, (b) Delay associated with the cross–correlation maximum at each site bar indicating ±2 milliseconds.

seen for time delays less than 5 timesteps or 0.5 milliseconds. For a 2000 Hz or less sampling system this would appear as zero–lag cross–correlation in agreement with Eckhorn and others [13].

The findings of zero–lag synchrony in the simplified averaging model, show nonlinear phase–locked oscillations are not needed for production of positive cross–correlations; only a system of coupled linear elements with delay summation on previous state values and connectivity with delay according to distance is necessary. In opposition to the conjectures of some authors [17, 18, 58] inhibitory elements are not required.

4.2. The physiological model

An examination of the physiological model was carried out to study the impact of local feedback dynamics upon synchronisation. In all cases correlations were obtained from LFP, and pulse–density results are equivalent.

In the standard two–input case of the complete model, nonspecific input Q_{ns} DC of 20.0 was input to all elements of the lattice while the driving sites on row eleven of the lattice in columns 8 and 14 each received Q_s Gaussian white noise signals of zero mean and standard deviation 0.005 to excitatory and inhibitory cell dendritic junctions. Multichannel time series of length 20000 points were acquired after an initialisation, and cross–correlation analysis carried out as before.

As for the Simplifed Averaging case a pattern of maximum cross–correlation (in the range 0.7–1.0) for delays of less than 5 timesteps (0.5 milliseconds) exists as a field surrounding the driving sites. See Figure 2.

4.2.1. Spatial dependencies of eigenvectors
PCA was employed to study global cooperative modes in both Simplified Averaging and Physiological models with the results in the synchrony ranges being illustrative of the same phenomena. Therefore only the physiological model PCA is presented here.

Driving sites were removed prior to analysis to facilitate viewing of the spatial field patterns. A 20000 length PCA was chosen from a study of the asymptotic properties of the eigenvalues and is discussed elsewhere [8]. Ensemble averages were taken to obtain standard errors on the variance associated with each mode. For a selection of noise seeds, the ensemble average of results over 25 runs are in Figure 3.

Two dominant modes, containing over 99% of the variance of the original multichannel signal, were found. The first mode was similar to the pattern of zero–lag cross–correlation in Figure 1; the second mode consisted of two lobes with opposite sign loadings. The first eigenvector had associated variance about four times the second's. Third and higher modes had significantly smaller eigenvalues and will not be examined.

4.2.2. Odd and even components of input signal
To discover what caused the dominant modes, two input paradigms were investigated. Firstly, two identical noise signals were fed to the driving sites – the
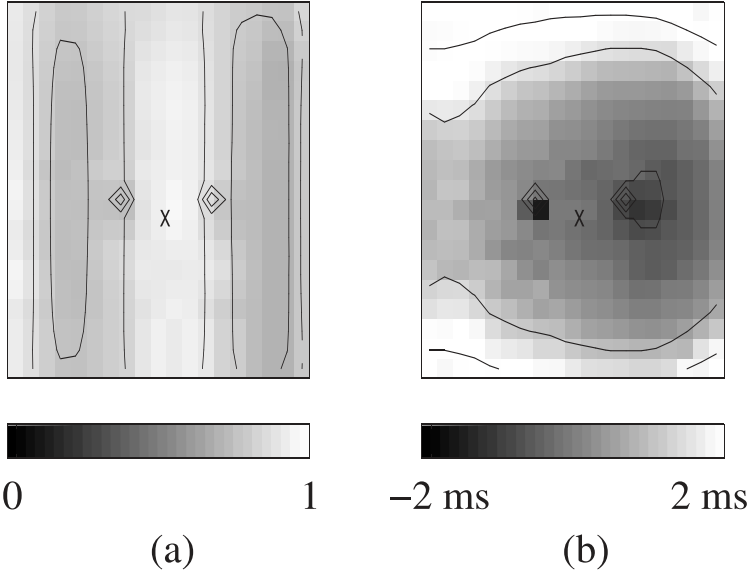
Fig. 2. Cross–correlation results.Physiological model 20 x 20 lattice with toroidal boundary conditions. Two specifically driven input sites (see text) received Gaussian mean zero white noise. Non–specific cortical activation (Q_{ns}) set at 20.0.(a) Grey scale spatial plots of maximum cross–correlation, of the site marked 'x', with every other site for lags of ±100 timesteps, (b) Delay associated with the cross–correlation maximum at each site bar indicating ±2 milliseconds.

synchronous noise case. Secondly, the same noise signals were input to both sites with the input to one channel multiplied by minus one – the *anti–synchronous* noise case. This amounted to inputting the even components of the two–dimensional noise signal for the former and the odd components of the same signal for the latter.

With purely synchronous or antisynchronous inputs, the ensemble eigenvectors (eigenmodes) are explained by odd and even components in the twin driving inputs. See Figure 3. In the synchronous noise case the first eigenmode occupies 99% of the variance and has the spatial form of the first mode in the asynchronous case. In the antisynchronous case the first eigenmode occupies 99% of the variance and has the spatial form of the second mode in the asynchronous case. The asynchronous case can then be explained by dominance of a synchronous eigenmode over an antisynchronous so the system acts as a coincidence detector; enhancing the transiently correlated inputs in the two noise signals, while reducing the effect of the negatively correlated ones. This process is made possible by dendritic summation in the elements.

The temporal characteristics of the synchronous field were examined using the the principal mode time evolutions. Ensemble averaged spectra of these evolutions in Figure 4, indicate movement to the right through the different designated EEG frequency bands as cortical activation (Q_{ns}) was increased. A similar shift in power

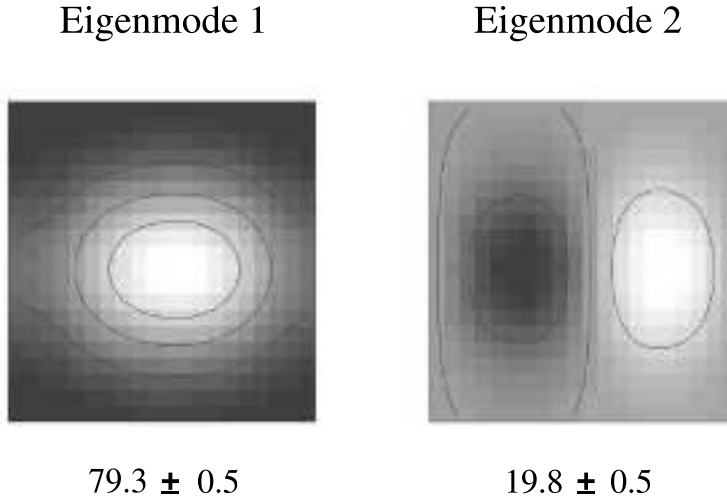# Eigenmode 1   Eigenmode 2

79.3 ± 0.5   19.8 ± 0.5

Fig. 3. First two ensemble averaged eigenvectors for 25 different noise seeds for PCA done over an interval of 20000 timesteps (2 seconds) on the 20 x 20 lattice simulation of Physiological model. Input and other conditions as for Figure 2. The numbers beneath the images indicate the percentage of variance associated with each eigenvector and the standard error on the basis of 25 runs.

spectra towards the gamma band has been found in animal experiments on the effect of increased reticular activation upon synchronous oscillations [39].

4.2.3. Effect of separation of sites on synchrony

Since coupling connectivity was a function of distance the effect of different separation of driving sites on synchrony was examined.

The physiological model was simulated on a 20 x 40 lattice to allow separation to an order of 19 intervening sites. Two sites situated symmetrically about the midline, and separated by 3 cells in row 11 of the lattice, were submitted to asynchronous Gaussian mean zero standard deviation 0.005 noise. The driven sites were then progressively moved apart and the multichannel output analysed with PCA.

Spatial eigenmodes for different driving site separations are in Figure 5. As separation increased the synchronous field broke down as first and second eigenmodes became two separate synchronous fields, one around each of the driving sites.

Additional coupling was employed to see if the fall–off of synchrony with distance was due to decreasing connection strength or the size of axonal time delays. The additional couplings were imposed between elements which were equal horizontal distances from the midline, and also declined in coupling strength with Gaussian distance. Standard axonal time delays were retained.

The dominant synchronous mode in this case retained the same concurrent fields of synchrony around both driving sites, and the first and second eigenmodes still partitioned responses to even and odd parts of the input signals. The first mode occupied a greater percentage of the variance than in the system with standard Gaussian
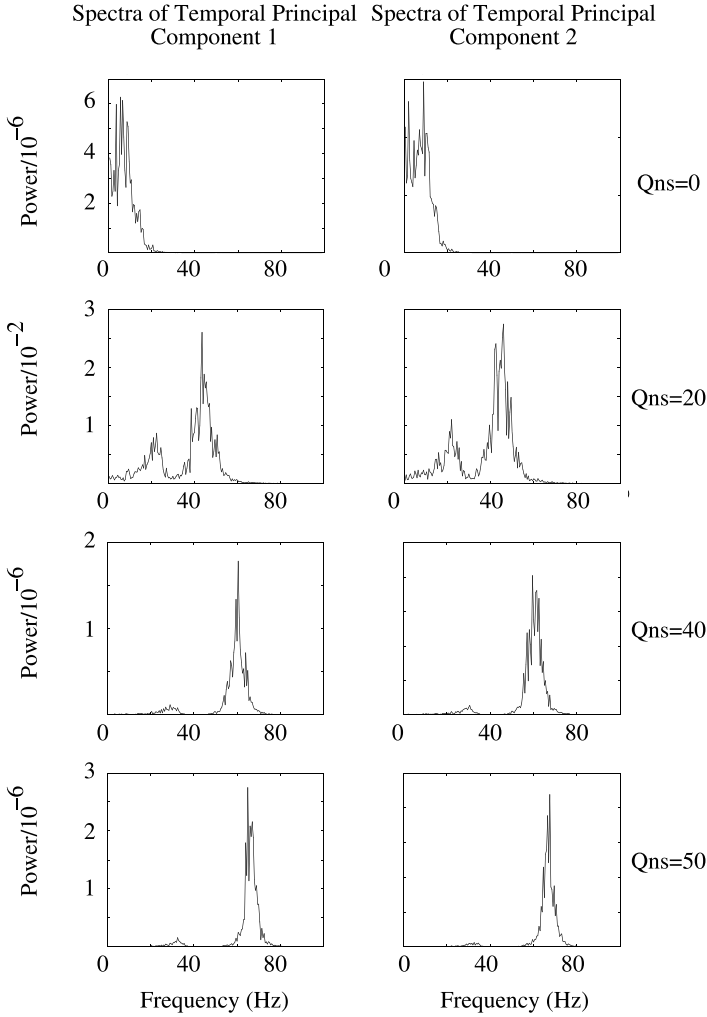
Spectra of Temporal Principal   Spectra of Temporal Principal
         Component 1   Component 2

Fig. 4. Power spectra of first two temporal principal component vectors associated with the eigenmodes in Figure 3. Ordered from top to bottom, $Q_{ns} = 0$, $Q_{ns} = 20$, $Q_{ns} = 40$ and $Q_{ns} = 50$. Ensemble avergages over 10 runs. Simulation timestep is 0.1 ms.

coupling; evidence for the role of relative connection strength in synchrony. See Figure 6.

4.2.4. Time of onset of synchrony in physiological model

If synchrony is in fact an important mediator of perceptual binding, then physiologically and in any plausible candidate model, the field of synchrony must be capable of flexible adaptation on a time–scale of milliseconds. Since perceptual coding is on
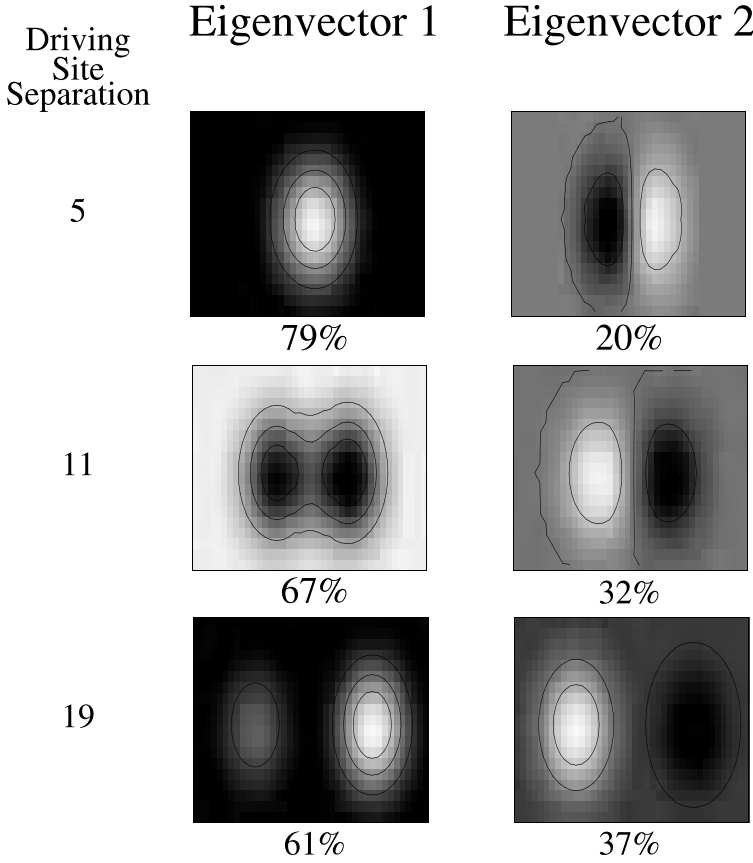
Fig. 5. First two eigenvectors and associated variances for PCA done over a 10000 timestep (1 second) interval of a 20 x 40 lattice simulation of the Physiological model. Two specifically driven input sites were located at separations of 5,11 and 19 intervening elements with $Q_{ns} = 20.0$ and $Q_s = 0.005$ standard deviation Gaussian mean zero white noise. Standard Gaussian coupling between sites was employed.

the order of a few milliseconds [2, 26, 29, 31, 38, 49, 55, 61] the temporal evolution of the system eigenmodes was studied.

A two–dimensional asynchronous noise signal was input as before, with Q_{ns}, of 20.0 to all elements. A repetition of the simulation was carried out for a matching signal, except for an aberrant 100 step (10 millisecond) noise signal at 15000 steps (1.5 seconds). The aberrant period had the same first order properties of mean and autocorrelation but was phase–randomised using the method of surrogate data [50].

After removal of a 5000 timestep initialisation, PCA was applied over 20000 timesteps and the principal component temporal vectors calculated for both 'normal' and 'aberrant' input cases using equation (5). The temporal evolution associated with the first eigenvector was studied since it contained the dominant spatial synchronous effect (similar results were found for higher order modes). The
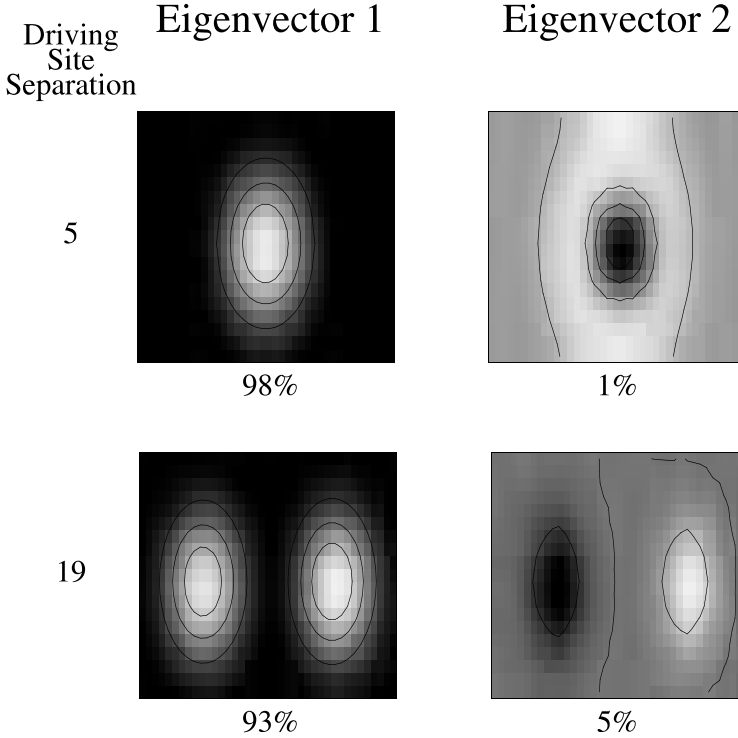
Fig. 6. First and second eigenmodes and associated variances for PCA done over a 10000 timestep (1 second) interval of a 20 x 40 lattice simulation of the Physiological model. Two specifically driven input sites were located at separations of 5 and 19 intervening elements with $Q_{ns} = 20.0$ and $Q_s = 0.005$ standard deviation Gaussian mean zero white noise as in Figure 5. Here both Standard Gaussian coupling and extra Long–range Gaussian coupling between sites was employed.

magnitude of the difference between the normal and aberrant times series was calculated. This procedure was repeated twenty–five times for a selection of pairs of noise signals. An ensemble average of the *magnitude of the difference* between the two series was then found. See Figure 7.

The aberrant noise input was taken to have been registered by the spatial field of the lattice when the magnitude of the difference between the two time series became *large*. Large, in this context, meant the change in *magnitude of the difference* at a given time point was larger than the maximum deviation from the mean observed at any time point in the 10000 *magnitude of the difference time series* before the aberrant noise onset.

A separation in the two temporal evolutions occurred at about 25–30 timesteps. See Figure 7. The synchronous field of the entire system will therefore respond to a different stimulus within a few milliseconds. Much smaller sections of the lattice respond even faster because of their closer connection proximity to the source.
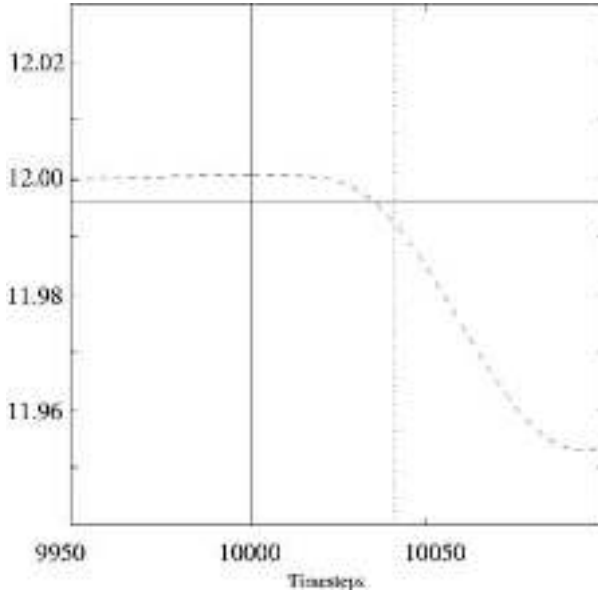
Fig. 7. Time taken to separate the two principal component temporal trajectories calculated for the system under two noise cases described in the text. Plot of magnitude of difference of two standardised series as a function of time '- -'. Vertical axes is in standardised units. The point at which the noise input to the two lattices became different is indicated in the diagram as a solid vertical line. The dotted '.' vertical line indicates 40 timesteps after the change in noise input. Where the dashed '- -' curve crosses the solid horizontal line indicates when the deviation became "large" as defined in text.

4.2.5. Nonlinear phase-locking results

If the level of non–specific input (Q_{ns}) was increased sufficiently to the two driving sites then each element in the system attained limit cycle oscillations. In particular, a state was obtained in which the elements of the lattice started to oscillate at a frequency close to 40 Hz.

As a first step, the phase relationships between the individual oscillating elements in the lattice were examined. The driving sites were completely phase–locked and locking was also found between other elements at a lag to the driving sites. A graph of the phase difference between the left–most driving site and every other element in the lattice is in Figure 8. Segments of the lattice were found to be phase–locked as expected for a time-delay nonlinear oscillator network. The operation of the wave mechanism described earlier allows phase–locking of outer array elements at a large phase lag to the driving sites. A similar phenomena of segregated phases has been found in a global system of nonlinear oscillators [60].

These oscillations were linked in zero–lag phase with other elements to form clusters of zero–lag phase and required local inhibition for their occurrence – in agreement with abstract nonlinear models of synchronous oscillation proposed by others [17, 18, 58].
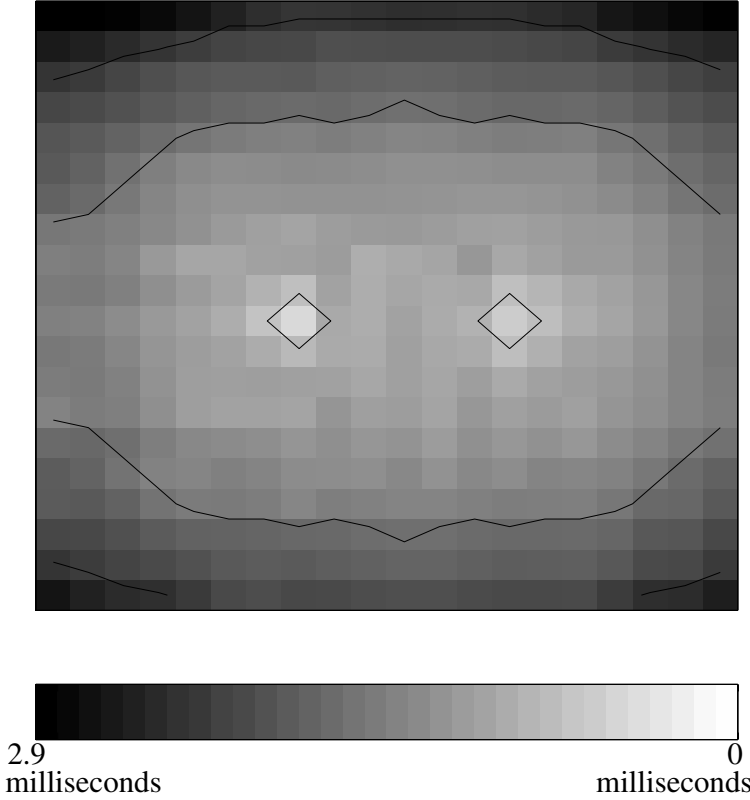
Fig. 8. Phase relationships between the left hand driving site and every other element of the lattice at a stage in which limit cycle oscillations are present. $Q_{ns} = 50$.

As Q_{ns} was increased the temporal evolution of individual lattice elements underwent transitions from damped or stable focus states through limit cycles to unstable foci. See Figure 9 for a selection of such transitions for one of the elements.

Complex periodic behaviour associated with a synchronous spatial field, similar to in the simple periodic case, was observed for lower level input driving and high values of Q_{ns}.

A qualitative check was made on how sensitive the limit cycle synchronous modes were to the input of noise. It was found the system remained stable even for relatively large noise inputs (standard deviation of 0.1) when Q_{ns} was 40 and Q_s was 0.6. The noise perturbed the system in and out of exact phase–locking but did not lead to completely uncontrolled excitation. The time course of two elements is in Figure 10.

The results are reminiscent of stable limit cycles with stochastic or nonlinear bursting seen in some physiological conditions [19, 20] and thought to be associated with specific perceptual events. The very limited use of complex neurotransmitter regulation in the present model precludes close comparison.
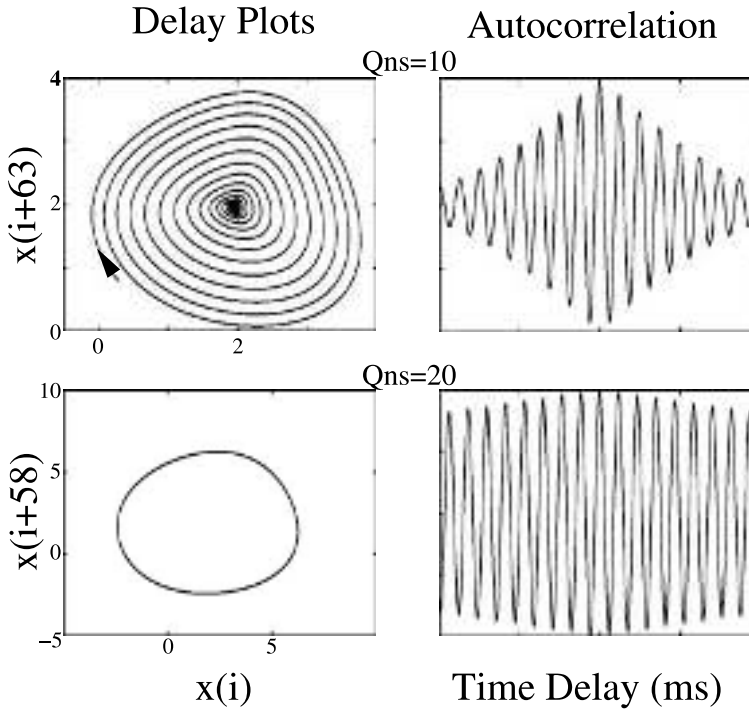
Fig. 9. Typical element temporal delay plots for voltage output x(i) vs lagged voltage output x(i+lag) from driving site 208 for various Q_{ns} values. Driving sites 208 and 214 received $Q_s = 0.8$. The top row shows stable focus behaviour and the bottom row a periodic orbit.

5. Discussion and conclusions

The results obtained in these simulations indicate synchronisation, between separated sites in the brain, may arise via fairly distinct mechanisms dependent on the level of cortical activation.

Firstly, synchrony is an inevitable property of delay elements similar to dendrites joined by long–range couplings with relatively rapid transmission and can be explained by simple linear models operating on uncorrelated inputs such as the Simplified Averaging model employed here. There is no need to assume special co–incidence detection properties of dendritic membranes or complicated local dynamics to explain the way synchrony can lead to the elimination of asynchronous components in the activity of two concurrently firing sites in cortex. Instead, this property emerges directly from an eigenfunction decomposition of the travelling waves which radiate from the active sites. As a corollary, because of the almost linear superposition properties of travelling waves in this media, the basic principles of decomposition of eigenmodes illustrated above still hold for experiments with multiple uncorrelated inputs as reported in a following paper [9]. Synchrony can be associated with rhythmic broad–band electrocortical activity, including that in the gamma band. It is also seen as damped autocorrelation and cross–correlation
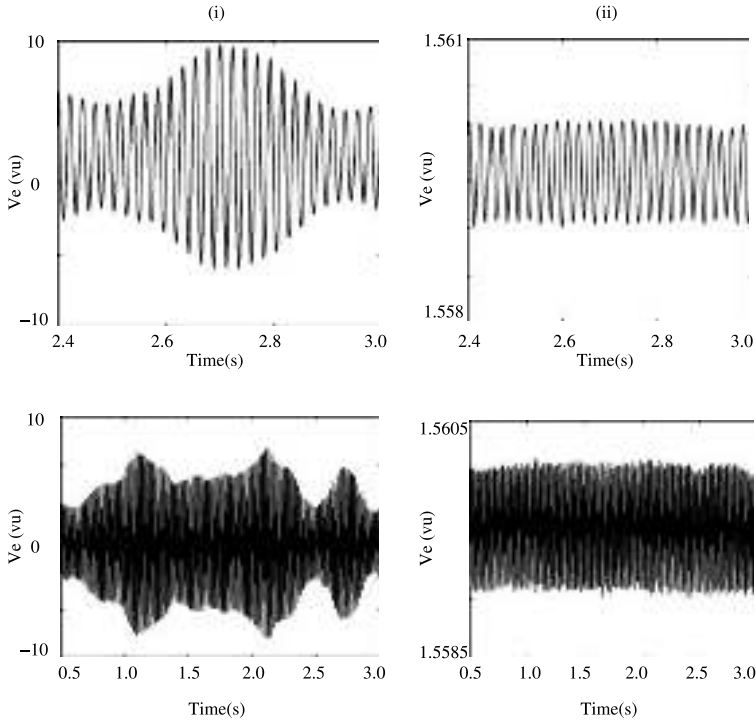
Fig. 10. Transitions from limit cycle to stochastic bursting with input of noise. Q_{ns} input of 40 and a Q_s DC of 0.6 with zero mean standard deviation 0.1 Gaussian white noise sent to driving sites 208 and 214 in a 20 x 20 lattice. Plots on the left–hand side are with respect to driving site 208 over different length time scales. Plots on the right–hand side are with respect to site 10 on the first row of the lattice, over different length time scales.

functions. The onset of synchrony via this mechanism can co–ordinate events in an extended neuronal field very rapidly, and is therefore well suited to the role of mediation of binding in cognitive and perceptual processes. This synchrony is quite distinct from oscillation – the oscillation arising locally and requiring local excitatory/inhibitory interactions – while synchrony requires only excitatory processes. Synchrony can arise over both long and short ranges, but the form of the synchronous field is sensitive to the specific coupling within the field. Specific corticocortical connections might provide a histological counterpart to the additional long–range connections employed in these situations [3, 21, 22]. Such connections have been associated in the visual cortex with similar receptive fields and orientation preference properties in spatially separated sites [28] that give rise to synchrony at distances up to 7 mm [23].

Secondly, at sufficiently high levels of activation of the physiological model, a nonlinear mechanism with phase–locking emerges. This mechanism is potentially capable of mediating much more complicated dynamic interactions between cortical sites. Oscillation and both excitatory and inhibitory synaptic transmission are essential to the mediation of this type of synchronisation. This may be equated

with the role in image segmentation ascribed to synchronous mechanisms in some models [10]. Notably, this synchronous mechanism could be partially distinguished from the former type by the cross–correlation and autocorrelation functions which it gives rise to. These functions would be virtually undamped for at least a transient period, and bandwidth limited (the 40 Hz band in this model), rather than broad–band.

Of the two mechanisms, the former linear synchrony would be much more readily observable physiologically, wherever large fields of cells interact regardless of scale. This may explain why broad–band synchrony is observed widely over many cortical areas [4]. The nonlinear mechanism would be seen only episodically and strictly locally, and may arise only in circumstances in which new information is emerging from autonomous local activity in the brain, rather than with the binding of simple sensory and perceptual information. These distinctions, although plain enough in simulation, are unlikely to be readily apparent physiologically. For instance, small changes in model parameters (which quantify more complex processes likely to be slowly time–varying in physiological reality) might shift the frequency of the nonlinear oscillation somewhat. Also, a distinction between noise–perturbed limit cycles and lightly damped linear oscillations in the gamma range cannot readily be made either on auto/cross–correlation profiles or with any other time series method – particularly since these separate dynamic processes may both occur transiently in the same recordings. First steps toward empirically distinguishing the two types of synchronisation using rotated PCA are reported in a following paper [9].

References

1. Abarbanel, H.D.I., Rabinovich, M.I., Selverston, A., Bazhenov, M.V., Huerta, R., Sushchik, M.M., Rubchinskiǐ, L.L.: Synchronization in Neural Networks. Physics-Uspekhi, **39**(4), 337–362 (1996)
2. Bair, W., Koch, C.: Temporal Precision of Spike Trains in Extrastriate Cortex of the Behaving Macaque Monkey. Neural Computation, **8**, 1185–1202 (1996)
3. Braitenberg, V., Schüz, A.: Anatomy of the Cortex: Statistics and Geometry. Berlin and New York: Springer–Verlag, 1991
4. Bressler, S.L., Coppola, R., Nakamura, R.: Episodic Multiregional Cortical Coherence at Multiple Frequencies During Visual Task Performance. Nature, **366**, 153–156 (1993)
5. Brosch, M., Bauer, R., Eckhorn, R.: Stimulus–Dependent Modulations of Correlated High–Frequency Oscillationsin Cat Visual Cortex. Cerebral Cortex, **7**, 70–76 (1997)
6. Brown, G., Wang, D.: Modelling the Perceptual Segregation of DoubleVowels with a Network of Neural Oscillators. The University of Sheffield, Department of Computer Science, 1996
7. Campbell, S., Wang, D.: Synchronization and Desynchronization in a Network of Locally Coupled Wilson-Cowan Oscillators. IEEE Transactions on Neural Networks, **7**, 541–554 (1996)
8. Chapman, C.L.: Investigation of Synchronisation in a Mathematical Model of Cortical Functionusing Principal Component Analysis. University of Sydney Australia, 1998
9. Chapman, C.L., Wright, J.J., Bourke, P.D.: Eigenvector Rotation Applied to Principal Components of Synchronisation in Simulated Cortex: Distinguishing Input Sources from Fields. In preparation, 2001

10. Chen, K., Wang, D.L.: A Dynamically Coupled Neural Oscillator Network for Image Segmentation. Department of Computer and Information Science and center for Cognitive Science, The Ohio State University, Columbus, OH 43210, USA, July 1998

11. Choi, M.Y.: Periodic Synchronization in Networks of Neuronal Oscillators. Seoul National University Theoretical Physics Preprints 95–015, (1995)

12. Destexhe, A., Babloyantz, A.: Pacemaker–Induced Coherence in Cortical Networks. Neural Computation, **3**, 145–154 (1991)

13. Eckhorn, R., Bauer, R., Jordan, W., Brosch, M., Kruse, W., Munkand, M., Reitboeck, H.J.: Coherent Oscillations: A Mechanism of Feature Linking in the Visual Cortex. Biological Cybernetics, **60**, 121–130 (1988)

14. Eckhorn, R., Reitboeck, H.J., Arndt, M., Dicke, P.: A Neural Network for Feature Linking via Synchronous Activity: Results from Cat Visual Cortex and from Simulations. In R.M.J. Cotterill, editor, Models of Brain Function, pages 255–272. Cambridge: Cambridge University Press, 1989

15. Engel, A.K., König, P., Kreiter, A.K., Singer, W.: Interhemispheric Synchronization of Oscillatory Neuronal Responses in Cat Visual Cortex. Science, **252**, 1177–1179 (1991)

16. Engel, A.K., Roelfsema, P.R., Fries, P., Brecht, M., Singer, W.: Binding and Response Selection in the Temporal Domain — a New Paradigm for Neurobiological Research. Theory of Biosciences, **116**, 241–266 (1997)

17. Ermentrout, B.: Complex Dynamics in Winner–Take–All Neural Nets with Slow Inhibition. Neural Networks, **5**, 415–431 (1992)

18. Ernst, U., Pawelzik, K., Geisel, T.: Synchronization Induced by Temporal Delays in Pulse–Coupled Oscillators. Physical Review Letters, **74**, 1570–1573 (1995)

19. Freeman, W.J., van Dijk, B.W.: Spatial Patterns of Visual Cortical Fast EEG During Conditioned Reflex in a Rhesus Monkey, Brain Research, **422**, 267–276 (1987)

20. Freeman, W.J.: Mass Action in the Nervous System New York: Academic Press, 1975

21. Gilbert, C.D., Wiesel, T.N.: Clustered Intrinsic Connections in cat visual cortex. Journal of Neuroscience, **3**, 1116–1133 (1983)

22. Gilbert, C.D., Wiesel, T.N.: Columnar Specificity of Intrinsic Horizontal and Corticocortical Connections in Cat Visual Cortex. Journal of Neuroscience, **9**, 2432–2442 (1989)

23. Gray, C., König, P., Engel, A., Singer, W.: Oscillatory Responses in Cat Visual Cortex Exhibit Inter–Columnar Synchronization which Reflects Global Stimulus Properties. Nature, **338**, 334–337 (1989)

24. Gray, C., Singer, W.: Stimulus–Specific Neuronal Oscillations in Orientation Columns of Cat Visual Cortex. Synchronization in Neural Networks, **86**, 1698–1702 (1989)

25. Gray, C.M., Viana Di Prisco, G. Stimulus–Dependent Neuronal Oscillations and Local Synchronization in Striate Cortex of the Alert Cat. The Journal of Neuroscience, **17**, 3239–3253 (1997)

26. Hirsh, I.J.: Auditory Perception of Temporal Order: The Journal of the Acoustical Society of America, **31**, 759–767 (1959)

27. Hodgkin, A.L., Huxley, A.F.: A Quantitative Description of Membrane Current and its Application to Conduction and Excitation in Nerve. Journal of Physiology, **117**, 500–544 (1952)

28. Hubel, D.H., Wiesel, T.N.: Functional Architecture of Macaque Monkey Visual Cortex. Proceedings Royal Society of London B, **198**, 1–59 (1977)

29. Joliot, M., Ribary, U., Llinás, R.: Human Oscillatory Brain Activity near 40 Hz Coexistswith Cognitive Temporal Binding. Proceedings National Academy of Science USA, **91**, 11478–11751 (1994)

30. Kandel, E.R., Schwartz, J.H.: Principles of Neural Science Second Edition. New York, Amsterdam, London: Elsevier, 1995

31. König, P., Engel, A.K., Roelfsema, P.R., Singer, W.: How Precise is Neuronal Synchronization? Neural Computation, **7**, 469–485 (1995)
32. König, P., Schillen, T.B.: Stimulus–Dependent Assembly Formation of Oscillatory Responses: I. Synchronization. Neural Computation, **3**, 155–166 (1991)
33. Liley, D.T.J., Wright, J.: Intracortical Connectivity ofPyramidal and Stellate Cells: Estimates of Synaptic Densities and Coupling Symmetry. Network, **5**, 175–189 (1994)
34. Livingstone, M.: Oscillatory Firing and Interneuronal Correlations in Squirrel Monkey Striate Cortex. Journal of Neurophysiology, **75**, 2467–2485 (1996)
35. Lumer, E.D., Edelman, G.M., Tononi, G.: Neural Dynamics in a model of the thalamocortical system. I. Layers, loops and the emergence of fast synchronous rhythms. Cerebral Cortex, **7**, 207–227 (1997)
36. Lumer, E.D., Edelman, G.M., Tononi, G.: Neural Dynamics in a Model of the Thalamocortical System. I. The Role of Neural Synchrony Tested Through Perturbations of Spike Timing. Cerebral Cortex, **7**, 228–236 (1997)
37. Marsaglia, G., Zaman, A.: Towards a Universal Number Generator. Technical Report FSU–SCRI–87–50, Florida State University, 1987
38. Miller, G.A., Taylor, W.G.: The Perception of Repeated Bursts of Noise. The Journal of the Acoustical Society of America, **2**, 171–182 (1948)
39. Munk, M.H.J., Roelfsema, P.R., König, P., Engeland, A.K., Singer, W.: Role of Reticular Activation in the Modulation of Intracortical Synchronization. Science, **272**, 271–274 (1996)
40. Neuenschwander, S., Singer, W.: Long–range Synchronisation of Oscillatory Light Responses in the Cat Retina and Lateral Geniculate Nucleus. Nature, **379**, 728–733 (1996)
41. Noell, K.-L., Weber, H.: Algorithm 712 Collected Algorithms from ACM. Transactions on Mathematical Software, **18**, 434–435 (1992)
42. Nunez, P.L.: Neocortical Dynamics and Human EEG Rhythms. New York, Oxford: Oxford University Press, 1995
43. Palm, G., Wennekers, T.: Synchronicity andits Use in the Brain. Behavioral and Brain Sciences, **20**, 695–696 (1997)
44. Rennie, C.J., Robinson, P.A., Wright, J.J.: Effects of Local Feedback on Dispersion of Electrical Waves in the Cerebral Cortex. Physical Review E, (In press), 1998
45. Rennie, C.J., Wright, J.J., Robinson, P.A.: Mechanisms of Cortical Electrical Activation and Emergence of Gamma Rhythm. J. Theo. Biol., (In press), 2000
46. Robinson, P.A., Rennie, C.J., Wright, J.J.: Propagation and Stability of Waves of Electrical Activity in the Cerebral Cortex. Physical Review E, **56**, 826–840 (1997)
47. Robinson, P.A., Rennie, C.J., Wright, J.J., Bahramali, H., Gordon, E., Rowe, D.L.: Prediction of Electroencephalographic spectra from Neurophysiology. Physical Review E, (submitted), 2000
48. Robinson, P.A., Wright, J.J., Rennie, C.J.: Synchronous Oscillations in the Cerebral Cortex. Physical Review E, **57**, 4578–4588 (1998)
49. Rolls, E.T., Tovee, M.J.: Processing Speed in the Cerebral Cortex and the Neurophysiology of Visual Masking. Proceedings Royal Society of London B, **257**, 9–15 (1994)
50. Schiff, S., Sauer, T., Chang, T.: Discriminating Deterministic Stochastic Dynamics in Neuronal Activity. Integrative Physiological and Behavioral Science, **29**, 246–261 (1994)
51. Segev, I.: Dendritic Processing. The Handbook of Brain Theory and Neural Networks, pages 282–289. Cambridge, Mass., London, England: MIT Press, 1995
52. Sompolinsky, H., Golomb, D., Kleinfeld, D.: Global Processing of Visual Stimuli in a Neural Network of Coupled Oscillators. Proceedings National Academy of Science USA, **87**, 7200–7204 (1990)

53. Thomson, A.M.: Activity–Dependent Properties of Synaptic Transmission at Two Classes of Connections made by Rat Neocortical Pyramidal Axons *in vitro*. Journal of Physiology, **502**, 131–147 (1997)
54. Thomson, A.M., West, D.C., Hahn, J., Deuchars, J.: Single Axon IPSPs Elicited in Pyramidal Cells by Three Classes of Interneuronesin Slices of Rat Neocortex. Journal of Physiology, **496**, 81–102 (1996)
55. Thorpe, S., Fize, D., Marlot, C.: Speed of Processing in the Human Visual System. Nature, **381**, 520–522 (1996)
56. Traub, R.D., Jeffreys, J.G.R., Whittingtonand, M.A., Jefferys, J.G.R.: Simulation of Gamma Rhythms in Networks of Interneurons and Pyramidal Cells. J. Computat. Neurosci., **4**, 141–150 (1997)
57. Traub, R.D., Whittington, M.A., Stanford, I.M., Jefferys, J.G.R.: A mechanism for generation of loing-range synchronous fast oscillations in the cortex. Nature, **383**, 621–624 (1996)
58. van Vreeswijk, C., Abbott, L.F., Ermentrout, G.B.: When Inhibition not Excitation Synchronizes Neural Firing. Journal of Computational Neuroscience, **1**, 313–321 (1994)
59. von der Malsburg, C., Schneider, W.: A Neural Cocktail–Party Processor. Biological Cybernetics, **54**, 29–40 (1986)
60. Wang, D.: Object Selection Based on Oscillatory Correlation. Department of Computer and Information Science and Center for Cognitive Science, The Ohio State University, Columbus, Ohio 43210, USA, **12**, 1996
61. Wennekers, T., Palm, G.: On the Relation Between Neural Modelling and Experimental Neuroscience. Theory of Biosciences, **116**, 267–283 (1997)
62. Whittington, M.A., Traub, R.D., Jefferys, J.G.R.: Synchronized Oscillations in Interneuron Networks Driven by Metabotropic Glutamate Receptor Activation. Nature, **373**, 612–615 (1995)
63. Wilson, H.R., Cowan, J.D.: Excitatory and Inhibitory Interactions in Localized Populations of Model Neurons. Biophysical Journal, **12**, 2–24 (1972)
64. Wilson, H.R., Cowan, J.D.: A Mathematical Theory of the Functional Dynamics of Cortical and Thalamic nervous Tissue. Kybernetik, **13**, 55–80 (1973)
65. Wright, J.J., Bourke, P.D., Chapman, C.L.: Synchronous Oscillation in the Cerebral Cortex and Object Coherence: Simulation of Basic Electrophysiological Findings. Biological Cybernetics, **83**, 341–353 (2000)
66. Wright, J.J., Robinson, P.A., Rennie, C.J., Gordon, E., Bourke, P.D., Chapman, C.L., Hawthorn, N., Lees, G.J., Alexander, D.: Toward an Integrated Continuum Model of Cerebral Dynamics: The Cerebral Rhythms Synchronous Oscillation and Cortical Stability. Biosystems, **63**, 71–88 (2001)
67. Wright, J.J.: EEG Simulation: Variation of Spectral Envelope Pulse Synchrony and $\approx$ 40 Hz Oscillation. Biological Cybernetics, **76**, 181–194 (1997)
68. Wright, J.J.: Simulation of EEG: Dynamic Changes in Synaptic Efficacy Cerebral Rhythms and Dissipative and Generative Activity in Cortex. Biological Cybernetics, **81**, 131–147 (1999)